Dalton Transactions

Accepted Manuscript

ROYAL SOCIETY OF CHEMISTRY

www.rsc.org/dalton

Journal Name

RSCPublishing

ARTICLE

A cheap and facile route to synthesize monodisperse magnetic nanocrystals and application as MRI agent

Cite this: DOI: 10.1039/x0xx00000x

Guixin Yang,[a] Fei He,[*,a] Ruichan Lv,[a] Shili Gai,[a] Ziyong Cheng,[b] Yunlu Dai,[a] and Piaoping Yang[*,a]

Received 00th January 2012,
Accepted 00th January 2012

DOI: 10.1039/x0xx00000x

www.rsc.org/

A facile solution-based thermal decomposition strategy, using very cheap polyisobutene succimide (PIBSI) and paraffin oil as surfactant and solvent, has been developed for the controllable synthesis of magnetic $MnFe_2O_4$ and $CoFe_2O_4$ nanocrystals (NCs) with high dispersibility, uniform shape, and high yield. By fine-tuning reaction temperature and growth time, the morphology and size of $MnFe_2O_4$ and $CoFe_2O_4$ NCs can be simply regulated. It is found that the surfactant PIBSI plays a key role in the final shape of the products due to its long chain with non-polar groups, which can markedly hinder the aggregation of the NCs and thus greatly improve the stability and dispersibility of the products. The results reveal that $MnFe_2O_4$ and $CoFe_2O_4$ NCs have good biocompatibility and obvious T_2 contrast enhancement effects have been achieved with the increase of iron concentration. $MnFe_2O_4$ and $CoFe_2O_4$ NCs show high longitudinal relaxivity of 165.6 and 65.143 mM^{-1} S^{-1} in aqueous solutions due to the positive signal enhancement ability of Fe^{3+} ions, indicating the highly potential to be used as effective T_2 contrast agents for magnetic resonance imaging (MRI).

1. Introduction

Due to the size-dependent electronic and magnetic properties, size-controlled nanocrystals (NCs) which may have potential applications in chemical sensors, catalysts, biological assay[1–10] and electrophotographic,[11,12] have gained great attention. Among the research of size-tunable NCs, great success has been achieved in the areas of transition metal oxides and salts,[13–15] which have rich magnetic properties due to the dominating role of anisotropy in magnetism.[16–19] For example, the magnetic performance of iron oxide is markedly influenced by the size and shape. To date, much effort has been devoted to the exploration of various approaches for the fabrication of magnetic NCs with diverse shape, size and dimensions,[20] because these NCs not only play a crucial role in above applications, but also can be used to enrich our understanding greatly.

While as a matter of fact, the study still has not got enough progress. For instance, among the diverse methods for the synthesis of magnetic NCs,[21–31] solvothermal synthesis,[9,25,26] hydrothermal method,[27–29] and thermal decomposition routes[30,31] are the most common ones. The hydrothermal method has many advantages such as low cost and good repeatability, but the disadvantages of poor size uniformity and large particle size greatly hinder its application.[32] Accordingly, the thermal decomposition method is a much better choice for synthesizing uniform magnetic NCs.[33–35] However, the used metal oxides precursors, surfactants and solvents are usually expensive and toxic,[36] which is still a major drawback for further technological application.[37,38] Therefore, searching nontoxic and inexpensive thermal decomposition routes should be highly promising.[1,39–42]

Hyeon and co-workers firstly developed the route to prepare metal oxide in octadecene using metal oleate as precursor and oleic acid as surfactant, which possess monodisperse spherical shape and tunable sizes.[43] From then on, more research using metal oleate in the shape-control of metal oxide NCs has been carried out. For example, Cao *et al.* also synthesized colloidal iron oxide NCs by a modified high temperature thermolysis process using 1-octadecene and 1-tetradecence as mixing solvent.[44] Fu *et al.* prepared uniform Fe_3O_4 NCs by thermal decomposition method.[30] The method has the advantages of high uniformity and easily scalable production. Guardia *et al.* synthesized cube-octahedral iron oxide NCs with different sizes by using $Fe(acac)_3$ as iron precursors in dibenzyl ether assisted by decanoic acid, and the particle size can be controlled by changing the amount of decanoic acid.[45] Sun and the co-workers used 1,2-hexadecanediol, oleic acid, oleylamine, and phenyl ether as surfactant and solvent to synthesize uniform $MnFe_2O_4$ NCs.[46] Dravld and co-authors synthesized uniform $CoFe_2O_4$ NCs by a high temperature thermolysis route using dodecylaine, lauric acid, 1,2-hexadecanediol, and benzyl ether as surfactant and solvent, and the MRI properties have also been studied.[47] However, the used surfactant and the solvent are expensive or toxic, which is still a major drawback for mass and green technological production. Furthermore, different from the extensive researches on Fe_3O_4 NCs, the synthesis of metal ferrite NCs with uniform shape and high dispersibility has much less been reported.[48] Thus, developing a cheap, nontoxic and mass production route for shape-controlled synthesis of these NCs should be highly desirable.

In this research, we developed a cheap and large-scale thermal decomposition method to produce $MnFe_2O_4$ and $CoFe_2O_4$ NCs using cheap PIBSI as surfactant and paraffin oil

as high boiling solvent. We synthesized as much as about 40 g of nanoparticles in a single reaction (Fig. S1), without a size-sorting process, which is obviously superior to the reported methods due to the markedly lower cost.[43,46,47] PIBSI is a very cheap and stable oil-soluble surfactant with two non-polar long chain tails and one polar head. It can overcome the drawback of the oleic-type surfactants with short molecular chains in shape controllable synthesis of NCs and markedly improve the compatibility of NCs. The nonpolar long chains can improve the dispensability and stability of the magnetic NCs, and the polar groups may make the surfactant adsorb well on the magnetic NCs. In addition, as the used high boiling solvent, paraffin oil is also very cheap and easily acquired. The shape and particle size of the products were tuned by altering the reaction time and temperature. In this way, $MnFe_2O_4$ and $CoFe_2O_4$ NCs with small particle size, good magnetic properties and high dispersion were achieved. Besides, magnetic nanoparticles are highly favoured in biomedical applications, such as magnetic resonance imaging (MRI), magnetic hyperthermia for cancer therapy, cells and DNA separation, and magnetically guided gene/drug delivery, due to their good stability and high biocompatibility with biological moieties.[49–52] To explore the application of the as-prepared NCs, the as-synthesized $MnFe_2O_4$ and $CoFe_2O_4$ NCs were chosen as magnetic hyperthermia agents for MRI T_2 measurement.

2. Experimental section

Chemicals and materials. Ferric chloride ($FeCl_3{\cdot}6H_2O$, 99%), manganese chloride ($MnCl_2{\cdot}4H_2O$, 99%), cobalt chloride ($CoCl_2{\cdot}4H_2O$, 99%), hexadecyl trimethyl ammonium bromide (CTAB), ethanol, oleic acid, sodium oleate, hexane were purchased from Sinopharm Chemical Reagent Co., Ltd. China. Polyisobutene succimide (PIBSI) and paraffin oil were purchased from China Petrochemical Corporation.

Synthesis of metal oleate precursors. The metal oleate complexes were prepared by a modified procedure. Typically, 40 mmol of manganese chloride ($MnCl_2{\cdot}4H_2O$, 99%) and 120 mmol of sodium oleate were dissolved in 60 mL of distilled water, 80 mL of ethanol and 140 mL of hexane in round-bottomed flask. Then the solution was heated at 70 °C for 4 h. After that, the solution was transferred into a separatory funnel. And the upper organic layer was separated and washed several times. The manganese oleate was produced by evaporating the remained hexane. Iron oleate and cobalt oleate complexes were synthesized in the same way.

Size-controlled synthesis of $MnFe_2O_4$ and $CoFe_2O_4$. 1 mmol of as-prepared $Mn(oleate)_2$ and 2 mmol of $Fe(oleate)_2$, 20 mL of paraffin oil and 0.2 g of PIBSI were mixed under magnetic stirring in N_2 atmosphere in a three-necked flask. The solution was firstly heated at 150 °C for 1 h, then raised to 310 °C and kept at this temperature for 2 h under N_2 flow with continuous stirring. Subsequently, the mixture was cooled to room temperature and the product was precipitated by the addition of ethanol, and finally dispersed in cyclohexane. $CoFe_2O_4$ NCs were prepared in the same route. The control experiments were carried out by changing the heating temperature (270 °C, 290 °C and 330 °C) and growth time (0.5 h, 1 h and 4 h) without adjusting other conditions.

Transferring into hydrophilic phase of oleic acid-stabilized $MnFe_2O_4$ and $CoFe_2O_4$ NCs. 2 mL of cyclohexane solution containing oleic acid-stabilized NCs (5–10 mg mL^{-1}) was mixed in 20 mL of water with 0.1 g of CTAB. The solution was then stirred vigorously to evaporate cyclohexane solvent at room temperature, leading to a clear and transparent water solution.

***In vitro* cytotoxicity of hydrophilic $MnFe_2O_4$ and $CoFe_2O_4$ NCs.** The *in vitro* cytotoxicity of hydrophilic $MnFe_2O_4$ (or $CoFe_2O_4$) NCs was determined by MTT (3–(4,5–dimethylthiazol–2–yl)–2,5–diphenyltetrazolium bromide) assay against L929 cells. First, L929 fibroblast cells were seeded in a 96-well plate at a density of 5000–6000 cells per well and cultured in 5% CO_2 at 37 °C, leaving 8 wells empty for blank controls. The hydrophilic $MnFe_2O_4$ NCs were sterilized by ultraviolet irradiation for 2 h, and then exposed to a series of $MnFe_2O_4$ concentrations of 7.8125, 15.625, 31.25, 62.5, 125, 250, and 500 μg mL^{-1} for another 24 h in 5% CO_2 at 37 °C, respectively. 5 mg/mL stock solution of MTT was prepared in PBS and was added to each well containing a different amount of NCs. After incubation in dark at 37 °C for 4 h, 100 μL of acidified isopropanol was added to each well, and shaken to thoroughly mix the formazan into the solvent. The absorbance of the suspension was recorded at 570 nm. The cell viability was determined by the equation: Cell viability (%) = $[A]_{test}/[A]_{control} \times 100\%$.

Characterization. X-Ray powder diffraction (XRD) patterns were obtained on a Rigaku TTR III diffractometer at a scanning rate of 10° min^{-1} in the 2θ range from 10° to 80°, using graphite monochromated Cu-Kα radiation (λ = 0.15405 nm). Transmission electron microscopy (TEM) and HRTEM (high resolution Transmission electron microscopy) were performed on a FEI Tecnai G2 S-Twin with a field emission gun at 200 kV. Images were digitally acquired on a Gatan multiple CCD camera. Magnetization measurements were carried out on a MPM5-XL-5 superconducting quantum interference device (SQUID) magnetometer at 300 K. IR measurement (KBr pellets) was performed on a Nicolet-magna FT-IR500. In Vitro T_2-weighted MR imaging experiments were carried out on a 0.5 T MRI magnet (Shanghai Niumai Corporation Ration NM120-Analyst). The hydrophilic $MnFe_2O_4$ samples were dispersed in water at different Fe concentrations determined by ICP-MS measurement. T_2 measurements were carried out using a nonlinear fit to changes in the mean signal intensity within each well as a function of the repetition time (TR) with a Huantong 1.5 T MR scanner.

3. Results and discussion

3.1. Phase, structure, and morphologies

Fig. 1 shows the XRD patterns of $MnFe_2O_4$ and $CoFe_2O_4$ prepared at 310 °C for 2 h, as well as the standard data of $MnFe_2O_4$ (JCPDS No. 10–0319) and $CoFe_2O_4$ (JCPDS No. 22–1086). It is found that the XRD patterns of the samples can be well indexed to the cubic $MnFe_2O_4$ and $CoFe_2O_4$ phases, respectively. No other peaks can be detected, indicating the high purity. The broad peaks reveals the nano-sized nature of the as-prepared NCs, which were used to calculate the crystallite sizes by Scherrer formula $D = 0.89\lambda/(\beta\cos\theta)$, where D is the average crystallite size, λ is the X-ray wavelength, and θ and β are the respective diffraction angle and full-width at half-maximum (FWHM). The mean crystallite size of $MnFe_2O_4$ and $CoFe_2O_4$ NCs are calculated to be 20 and 28 nm, respectively.

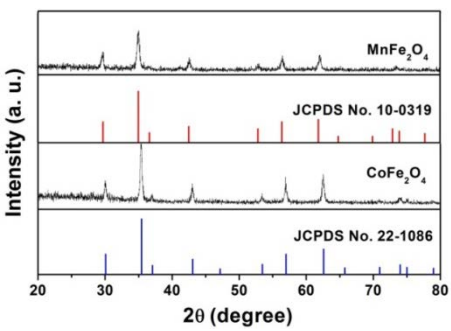

Fig. 1 XRD patterns of $MnFe_2O_4$ $CoFe_2O_4$ prepared at 310 °C for reaction time of 2 h, and the standard data of cubic $MnFe_2O_4$ (JCPDS No. 10–0319) and $CoFe_2O_4$ (JCPDS No. 22–1086).

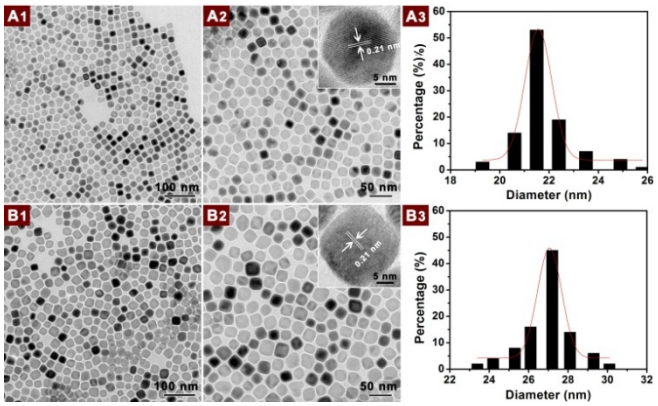

Fig. 2 TEM images with different magnification and the size distribution histograms of $MnFe_2O_4$ (A1-A3) and $CoFe_2O_4$ (B1-B3) NCs synthesized at 310 °C for 2 h. Insets are the corresponding HRTEM images.

The TEM images of as-prepared $MnFe_2O_4$ and $CoFe_2O_4$ NCs synthesized at 310 °C for 2 h are given in Fig. 2. It can be seen that all the samples consist of monodisperse NCs and the particle sizes of the three NCs are 21 and 27 nm, corresponding well to the XRD results. From the HRTEM image (inset, Fig. A2), we can clearly see the as-synthesized $MnFe_2O_4$ NCs are about 21 nm in size. The obvious lattice fringes indicate the high crystallinity of the sample, and the interplanner distance is determined to be 0.21 nm, matching well with the d_{200} spacing of cubic-phased $MnFe_2O_4$ (JCPDS No. 10–0319). In the size distribution histogram (Fig. 2A3), the sample shows relatively narrow particle size distribution. Similar HRTEM and particle size distribution results have been achieved for $CoFe_2O_4$ NCs (Fig. 2B).

In this study, PIBSI is used as surfactant, and the size of the NCs can be mainly controlled by the temperature and reaction time. In order to make clear the formation process of $MnFe_2O_4$ NCs, the temperature-dependent experiments were monitored were carried out. The TEM image (Fig. 3A) shows that highly dispersed $MnFe_2O_4$ NCs are obtained at 270 °C while the shape is irregular. In our study, the used paraffin oil is mainly composed of normal alkanes from C16 to C20, and the C18 alkane is most abundant component with the boiling point of 300 °C. It has been reported that one oleate ligand dissociated from the $M(oleate)_3$ precursor gives rise to the nucleation at 200–240 °C, while the growth occurs at about 300 °C triggered by the dissociation of the remained two oleate ligands.[43] Thus, the $M(oleate)_3$ precursor partially decomposed at 270 °C below the boiling point of the paraffin oil, yielding the highly dispersed NCs due to the dominant nucleation processes. However, the NCs cannot crystalize completely because of the low reaction temperature, resulting in the irregular shape

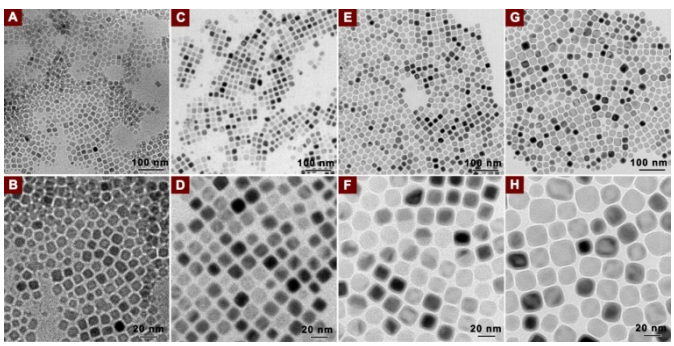

Fig. 3 TEM images of $MnFe_2O_4$ NCs synthesized for reaction time of 2 h at 270 °C (A, B), 290 °C (C, D), 310 °C (E, F), and 330 °C (G, H).

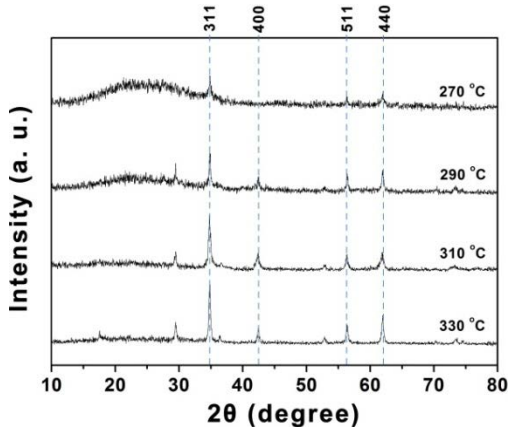

Fig. 4 XRD patterns of $MnFe_2O_4$ NCs synthesized for reaction time of 2 h at 270 °C, 290 °C, 310 °C and 330 °C.

(Fig. 3A, B). This can be also been proved by the XRD results. In the XRD pattern of the sample synthesized at 270 °C (Fig. 4), the obvious peaks at 34.98°, 42.527°, 56.2° and 61.7° correspond to the (311), (400), (511) and (440) planes of cubic $MnFe_2O_4$ (JCPDS No. 10–0319), while the broad peak centered at about 22° can be assigned to the un-decomposed $M(oleate)_3$ precursor. For the sample synthesized at 290°C, the crystallinity and the regular degree have been obviously enhanced. As discussed above, the sample synthesized at 310 °C above the boiling point of the liquid paraffin consists of monodisperse NCs with regular morphology (Fig. 3E, F), which should be attributed to the complete $M(oleate)_3$ decomposition induced homogenous nucleation. When further increasing the temperature to 330 °C, the sample shows increased crystallinity (Fig. 4) and some irregular size (Fig. 3G, H), which can be due to the growth and secondary nucleation at higher temperature. Moreover, the increased particle diameter of $MnFe_2O_4$ NCs with the increase of temperature can be explained by the higher reactivity of the manganese–oleate complex. And it is well accepted that high temperature is favourable for the transformation from small to large particle size in the solution-based procedure. The similar trends have also been observed for $CoFe_2O_4$ NCs (Fig. S2, S3).

With identical reaction temperature and surfactant amount, $MnFe_2O_4$ NCs with different sizes have also been synthesized by changing the reaction time. Fig. 5 shows the TEM images of cubic $MnFe_2O_4$ NCs prepared at 310 °C for different reaction time. It is found that NCs synthesized at 310 °C for 4 are not uniform, which may be due to the further growth. In previous reports, the average sizes of these NCs are almost similar no matter what reaction time is changed. However, in our study, alternation of the reaction time can indeed change the particle size. By increasing the reaction time, the mean size of $MnFe_2O_4$ NCs can be tuned from 18 nm (Fig. 4A, B),

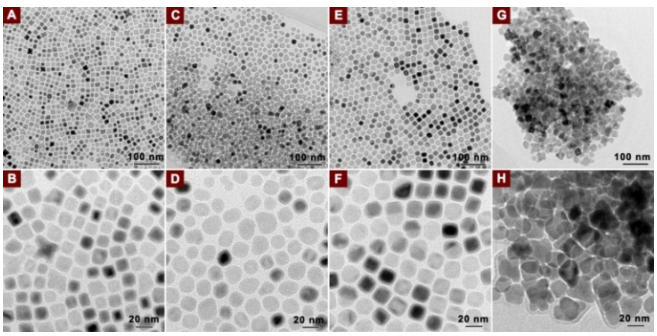

Fig. 5 TEM images of $MnFe_2O_4$ NCs synthesized at 310 °C for reaction time of 0.5 h (A, B), 1 h (C, D), 2 h (E, F), and 4 h (G, H).

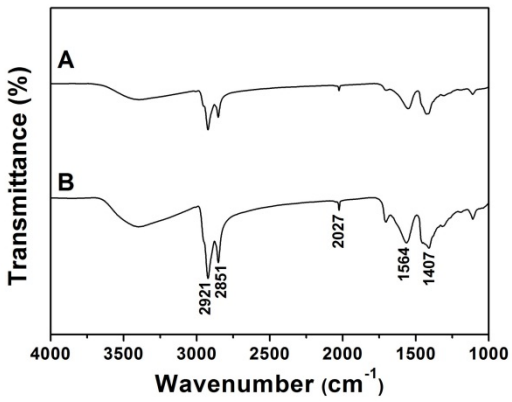

Fig. 6 FT-IR spectra of $MnFe_2O_4$ (A) and $CoFe_2O_4$ (B) NCs prepared at 310 °C for 2 h.

to 20 nm (Fig. 4C, D), and then to 21 nm (Fig. E, F). And the similar results have also been observed for $CoFe_2O_4$ NCs (Fig. S4). In a word, we can infer that tuning of the NCs diameter using thermal decomposition of metal oleate precursors can be achieved by simply changing the reaction temperature and the growth time of the NCs.

The functional groups on the surface of as-synthesized NCs were characterized by the FT-IR spectra, as shown in Fig. 6. The weak stretching mode of the -COOH group at 2027 cm^{-1} suggests the presence of trace amounts of free oleic acid on the surface of NCs. The bands at 1407 and 1564 cm^{-1} can be assigned to the antisymmetric and symmetric vibration modes of the $-COO^-$ group, showing the adsorption of oleic acid on the NCs surface through the bidentate bonds. Additionally, the peaks at 2921 and 2851 cm^{-1} can be associated with the stretching mode of $-CH_3$ and $-CH_3-$ groups, respectively.

3.2. Magnetic Properties

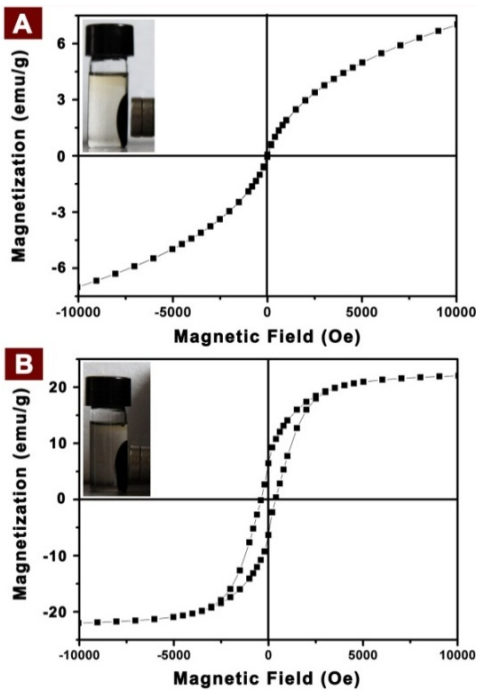

Fig. 7 Magnetizations of $MnFe_2O_4$ (A) and $CoFe_2O_4$ (B) as a function of applied magnetic field measured at room temperature. Insets are the corresponding magnetization photographs.

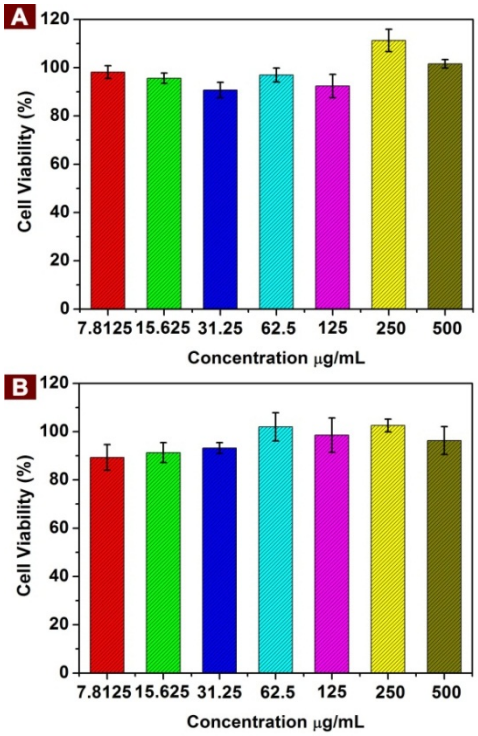

Fig. 8 The L929 cell viability after being incubated with different concentration of $MnFe_2O_4$ (A) and $CoFe_2O_4$ (B) NCs.

The field-dependent magnetizations of the as-synthesized $MnFe_2O_4$ and $CoFe_2O_4$ NCs measured at room temperature are shown in Fig. 7. And insets are their corresponding photographs of the magnetic colloid at hexane, which are colloidal dispersions of magnetic NCs. It is found from that the magnetization plots in Fig. 7 that $MnFe_2O_4$ and $CoFe_2O_4$ NCs are super paramagnetic with saturation magnetization value of 6.3 and 19.2 emu g^{-1}, respectively. The high saturation magnetizations of the $MnFe_2O_4$ and $CoFe_2O_4$ NCs make it potential to be used in the field of MRI measurement.

3.3. Biocompatibility and MRI measurement

It is well known that it is important to evaluate the biocompatibility of the sample for potential biomedical application. Standard MTT assay carried on L929 cell lines to detect the viability was performed. The cell viability as a function of the particle concentration incubated for 24 h is given in Fig. 8. It is apparent that all $MnFe_2O_4$ and $CoFe_2O_4$ NCs exhibit good biocompatibility in all dosages. Even incubated at high concentration of 500 μg/mL, the L929 cell viability is 101.6% and 96.32%, suggesting that the $MnFe_2O_4$ and $CoFe_2O_4$ NCs are very low toxic to L929 cells.

To verify the potential to be used as MRI contrast agents, $MnFe_2O_4$ and $CoFe_2O_4$ NCs were employed to conduct T_2-weighted magnetic resonance imaging with different iron concentrations (determined by ICP-MAX) at room temperature. Fig. 9A gives the concentration-dependent darkening T_2 effects of $MnFe_2O_4$ NCs. It is found that the as-obtained T_2-weighted images change obviously in signal intensity with the increase of the iron concentration. The relaxation rates R_2 ($1/T_2$) of the samples with different iron concentrations are given in Fig. 9B, D. We can see that the rate increases linearly with the iron concentrations, indicating that $MnFe_2O_4$ NCs generate MRI contrasts on T_2 weighted spin-echo sequences. The longitudinal relaxivity (r_2) value of $MnFe_2O_4$ NCs is calculated to be 165.6 mM^{-1} S^{-1}, indicating that the sample can be used as a

favourable T_2 contrast agent. T_2-weighted MR images of $CoFe_2O_4$ NCs with different iron concentrations at 25 °C and plot of T_2 relaxation rate ($1/T_2$) against iron concentration for $CoFe_2O_4$ NCs are displayed in Fig. 9C and Fig. 9D, respectively. Similar results are observed to those of $MnFe_2O_4$ NCs. And the longitudinal relaxivity (r_2) value of $CoFe_2O_4$ NCs is calculated to be 65.143 $mM^{-1} S^{-1}$.

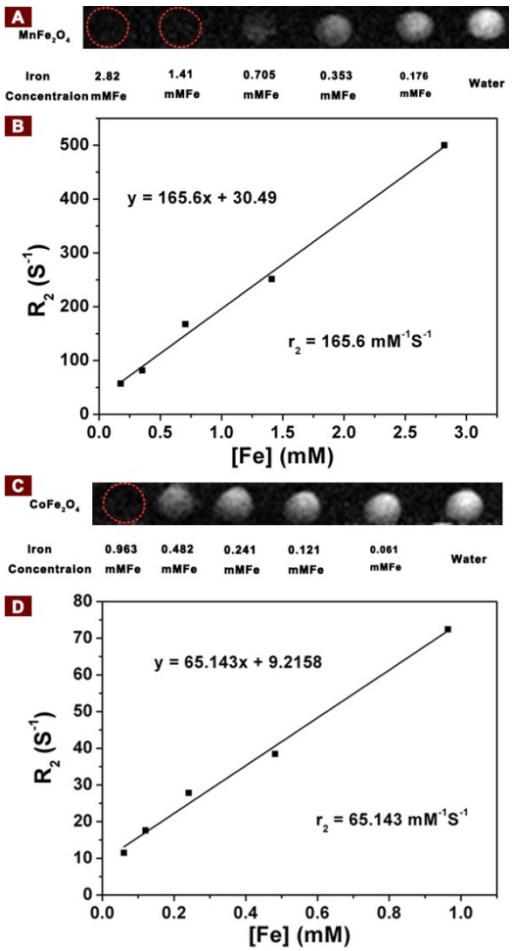

Fig. 9 T_2-weighted MR images of $MnFe_2O_4$ NCs with different iron concentrations at 25 °C (A), plot of T_2 relaxation rate ($1/T_2$) against iron concentration for $MnFe_2O_4$ NCs (B); $CoFe_2O_4$ NCs with different iron concentrations at 25 °C (C), plot of T_2 relaxation rate ($1/T_2$) against iron concentration for $MnFe_2O_4$ NCs (D).

4. Conclusions

In summary, we have demonstrated a very cheap, facile and mass-production method to synthesize monodisperse $MnFe_2O_4$ and $CoFe_2O_4$ NCs using cheap polyisobutene succimide as surfactant. All the as-synthesized NCs have uniform size, good dispersibility, and high saturation magnetization. Importantly, the size and shape of the as-synthesized NCs can simply be tuned by altering the reaction temperature and time. MTT assay shows the good biocompatibility of the sample. The T_2-weighted MR studies revealed that the $MnFe_2O_4$ and $CoFe_2O_4$ NCs are effective T_2 contrast agents, which are highly potential for various biomedical applications.

Acknowledgements

This work was supported by funding from financial supports from the National Natural Science Foundation of China (NSFC 21271053, 21401032, 51472058), Research Fund for the Doctoral Program of Higher Education of China (2011230411002, 2014M560248), Natural Science Foundation of Heilongjiang Province (LC2012C10, B201403), Harbin Sci.-Tech. Innovation Foundation (RC2012XK017012, 2014RFQXJ019) and Fundamental Research Funds for the Central Universities of China (HEUCF201403006).

Notes and references

a Key Laboratory of Superlight Materials and Surface Technology, Ministry of Education, College of Material Science and Chemical Engineering, Harbin Engineering University, Harbin 150001, P. R. China. E-mail: yangpiaoping@hrbeu.edu.cn; hefei1@hrbeu.edu.cn
b State Key Laboratory of Rare Source Utilization, Changchun Institute of Applied Chemistry, Chinese Academy of Sciences, Changchun, 130021, P. R. China

† Electronic Supplementary Information (ESI) available: [XRD patterns of $CoFe_2O_4$ NCs synthesized at 270 °C, 290 °C, 310 °C and 330 °C; TEM images of $CoFe_2O_4$ NCs synthesized at different temperatures; TEM images of $CoFe_2O_4$ NCs synthesized at 310 °C for different reaction time]. See DOI: 10.1039/b000000x/

1 L. J. Zhao, H. J. Zhang, Y. Xing, S. Y. Song. S. Y. Yu, W. D. Shi, X. M. Guo, H. H. Yang, Y. Q. Le and F. Cao, *Chem. Mater.*, 2008, **20**, 198-204.
2 H. X. Mai, Y. W. Zhang, R. Si, Z. G. Yan, L. D. Sun, L. P. You and C. H. Yan, *J. Am. Chem. Soc*., 2006, **126**, 6426-6436.
3 H. Lee, E. Lee, D. K. Kim, N. K. Jang, Y. Y. Jeong and S. Jon, *J. Am. Chem. Soc*., 2006, **128**, 7383-7389.
4 Y. S. Liu, D. T. Tu, H. M. Zhu and X. Y. Chen, *Chem. Soc. Rev.*, 2013, **42**, 6942-6958.
5 S. J. Zeng, M. K. Tsang, C. F. Chan, K. L. Wong and J. H. Hao, *Biomaterials* 2012, **33**, 9232-9238.
6 Y. Xiong, Y. Xie, S. Chen and Z. Li, *Chem.-Eur. J*., 2003, **9**, 4991-4996.
7 S. L. Gai, C. X. Li, P. P. Yang and J. Lin, Chem. Rev., 2014, **114**, 2343-2389.
8 X. Jia, D. Chen, X. Jiao, T. He, H. Wang and W. Jiang, *J. Phys. Chem. C*, 2008, **112**, 911-917.
9 M. L. Debasu, D. Ananias, S. L. C. Pinho, C. F. G. C. Geraldes, L. D. Carlos and J. Rocha, Nanoscale, 2012, *4*, 5154-5162.
10 S. G. Grancharov, H. Zeng, S. Sun, S. X. Wang, S. O'Brien, C. B. Murray, J. R. Kirtley and G. A. Held, *J. Phys. Chem. B*, 2005, **109**, 13030-13035.
11 D. Sarkar, M. Mandal and K. Mandal, *J. Appl. Phys*., 2012, **112**, 064318.
12 K. Baert, W. Libaers, B. Kolaric, R. A. L. Vallee, M. Van der Auweraer, K. Clays, D. Grandjean, M. Di Vece and P. Lievens, *J. Nonlinear. Opt. Phys*., 2007, **16**, 281-294.
13 S. Zhang, Y. Y. Shao, H. G. Liao, J. Liu, I. A. Aksay, G. P. Yin and Y. H. Lin, *Chem. Mater*., 2011, **23**, 1079-1081.
14 M. D'Arienzo, J. Carbajo, A. Bahamonde, M. Crippa, S. Polizzi, R. Scotti, L. Wahba and F. Morazzoni, *J. Am. Chem. Soc*., 2011, **133**, 17652-17661.
15 J. Zhao, Y. Cai, J. P. Yang, H. X. Wei, Y. H. Deng, Y. Q. Li, S. T. Lee and J. X. Tang, *Appl. Phys. Lett*., 2012, **101**, 193303.
16 S. J. Yoon, B. G. Kim, I. T. Jeon, J. H. Wu and Y. K. Kim, *Appl. Phys. Express.*, 2012, **5**, 103003.
17 J. Mohapatra, A. Mitra, D. Bahadur and M. Aslam, *CrystEngComm*, 2013, **15**, 524-532.
18 Q. Song and Z. J. Zhang, *J. Phys. Chem. B*, 2006, **110**, 11205-11209.

19 A. F. Rebolledo, A. B. Fuertes, T. Gonzalez-Carreño, M. Sevilla, T. Valdes-Solis and P. Tartaj, *Small*, 2008, **4**, 254-261.
20 T. S. Wang, Z. H. Liu, M. M. Lu, B. Wen, Q. Y. Ouyang, Y. J. Chen, C. L. Zhu, P. Gao, C. Y. Li, M. S. Cao and L. H. Qi, *J. Appl. Phys.*, 2013, **113**, 024314.
21 A. Abou-Hassan, S. Neveu, V. Dupuis and V. Cabuil, *RSC Adv*., 2012, **2**, 11263-11266.
22 S. H. Xuan, Y. X. J. Wang, J. C. Yu and K. C. F. Leung, *Chem. Mater*., 2009, **21**, 5079-5087.
23 G. Vaidyanathan, S. Sendhilnathan and R. Arulmurugan, *J. Magn. Magn. Mater*., 2007, **313**, 293-299.
24 R. Sani, A. Beitollahi, Y. V. Maksimov and I. P. Suzdalev, *J. Mater. Sci*., 2007, **42**, 2126-2131.
25 Y. Hou, J. Yu and S. Gao, *J. Mater. Chem*., 2003, **13**, 1983-1987.
26 S. Si, C. Li, X. Wang, D. Yu, Q. Peng and Y. Li, *Cryst. Growth Des*., 2005, **5**, 391-393.
27 J. Wang, Q. W. Chen, B. Y. Hou and Z. M. Peng, *Eur. J. Org. Chem*., 2004, 1165-1168.
28 X. Y. Hou, J. Feng, X. D. Xu and M. L. Zhang, *J. Alloys Compd*., 2010, **491**, 258-263.
29 M. Srivastava, S. Chaubey and A. K. Ojha, *Mater. Chem. Phys*., 2009, **118**, 174-180.
30 B. Bateer, C. G. Tian, Y. Qu, S. C. Du, T. X. Tan, R. H. Wang, G. H. Tian and H. G. Fu, *CrystEngComm*, 2013, **15**, 3366-3371.
31 H. X. Wu, G. Liu, X. Wang, J. M. Zhang, Y. Chen, J. L. Shi, H. Yang, H. Hu and S. P. Yang, *Acta Biomater*., 2011, **7**, 3496-3504.
32 A. Shavel, B. Rodríguez-González, J. Pacifico, M. Spasova, M. Farle and L. M. Liz-Marzán, *Chem. Mater*., 2009, **21**, 1326-1332.
33 L. M. Bronstein, J. E. Atkinson, A. G. Malyutin, F. Kidwai, B. D. Stein, D. G. Morgan, J. M. Perry and J. A. Karty, *Langmuir*, 2011, **27**, 3044-3050.
34 N. Bao, L. Shen, W. An, P. Padhan, C. Heath Turner and A. Gupta, *Chem. Mater*., 2009, **21**, 3458-3468.
35 Y. Wu, D. M. Yang, X. J. Kang, C. X. Li and J. Lin, *Mater. Res. Bull*., 2013, **48**, 2843-2849.
36 R. H. Kodama, *J. Magn. Magn. Mater*., 1999, **200**, 359-372.
37 H. G. Cha, C. W. Kim, S. W. Kang, B. K. Kim and Y. S. Kang, *J. Phys. Chem. C*, 2010, **114**, 9802-9807.
38 J. A. Gomes, G. M. Azevedo, J. Depeyrot, J. Mestnik-Filho, G. J. da Silva, F. A. Tourinho and R. Perzynski, *J. Magn. Magn. Mater*., 2011, **323**, 1203-1206.
39 L. Zhu, Y. Xu, W. Yuan, J. Xi, X. Huang, X. Tang and S. Zheng, *Adv. Mater*., 2006, **18**, 2997-3000.
40 J. Zhou, L. Meng and Q. Lu, *J. Mater. Chem*., 2010, **20**, 5493-5498.
41 Y. Li and M.-H. Xu, *Chem. Commun*., 2014, **50**, 3771-3782.
42 R. A. Brooks, *Magn. Reson. Med*., 2002, **47**, 388-391.
43 J. Park, K. J. An, Y. S. Hwang, J. G. Park, H. J. Noh, J. Y. Kim, J. H. Park, N. M. Hwang, T. Hyeon, *Nature Mat.* 2004, **3**, 891-895.
44 J. Lynch, J. Q. Zhuang, T. Wang, D. LaMontagne, H. M. Wu and Y. C. Cao, *J. Am. Chem. Soc.*, 2011, **133**, 12664-12674.
45 P. Guardia, N. Perez, A. Labarta, X. Batlle, *Langmuir*, 2010, **26**, 5843-5847.
46 H. M. Joshi, Y. P. Lin, M. Aslam, P. V. Prasad, E. A. Schultz-Sikma, R. Edelman, T. Meade and V. P. Dravid, *J. Phys. Chem. C*, 2009, **113**, 17761-17767.
47 S. H. Sun, H. Zeng, D. B. Robinson, S. Raoux, P. M. Rice, S. X. Wang and G. X. Li, *J. Am. Chem. Soc*., 2004, **126**, 273-279.
48 L. J. Zhao, H. J. Zhang, L. Zhou, Y. Xing, S. Y. Song and Y. Q. Lei, *Chem. Commun*., 2008, 30, 3570-3572.
49 A.-H. Lu, E. L. Salabas and F. Schüth, *Angew. Chem. Int. Ed*., 2007, **46**, 1222-1244.
50 S. Laurent, D. Forge, M. Port, A. Roch, C. Robic, L. Vander Elst and R. N. Muller, *Chem. Rev*., 2008, **108**, 2064-2110.
51 N. Lee and T. Hyeon, *Chem. Soc. Rev*., 2012, **41**, 2575-2589.
52 L. H. Reddy, J. L. Arias, J. Nicolas and P. Couvreur, *Chem. Rev.*, 2012, **112**, 5818-5878.

Monodisperse $MnFe_2O_4$ and $CoFe_2O_4$ nanocrystals (NCs) were synthesized by a facile thermal decomposition strategy, using very cheap polyisobutene succimide and paraffin oil as surfactant and solvent. The NCs could be used as effective T_2 contrast agent for magnetic resonance imaging (MRI).